Computer Assisted Mechanics and Engineering Sciences, **16**: 291–307, 2009.

Application of the Strongin-Sergeyev global optimization method in the compliance minimization of latticed shells

Sławomir Czarnecki
Faculty of Civil Engineering
Warsaw University of Technology
al. Armii Ludowej 16, 00-637 Warsaw, Poland
e-mail: czs@il.pw.edu.pl

(Received in the final form January 18, 2010)

The aim of the present paper is to revisit some known truss optimization problems by applying the genuine Strongin and Sergeyev's algorithm of the global search [8]. By employing the space-filling Hilbert-Peano-type curves, the wide class of non-convex and multidimensional constrained global optimization problems is reduced to one-dimensional ones. Then, the global minimum of the objective function in one-dimensional problem can be effectively found by means of Multivariate Index Method (MIM) that can be treated as a special version of one-dimensional Global Search Algorithm (GSA) over the set of open intervals adopted to constrained problems.

1. Introduction

Global optimization tools became very important components of effective algorithms in science, economics and engineering. Due to the existence of multiple local optima that differ from the global solutions, many problems in engineering design and control cannot be solved by classical nonlinear programming techniques. During the past few decades many new theoretical, algorithmic and computational tools of global optimization have been proposed and elaborated. We mention here only about few new ideas. The most popular algorithms base on statistical methods. The evolution and genetic algorithms (see e.g. [6]) are still regarded as the most effective and simple in implementation. Another very interesting branch of global optimization techniques has its source in real interval analysis [3]. More mathematically advanced methods base on Morse Theory, Karush-Kuhn-Tucker points and Chebyshev Approximation [4]. Yet another method of global optimization bases on very original idea of reducing multidimensional constrained optimization problems to one-dimensional ones. The foundation of this method is the theory of space-filling Hilbert-Peano-type curves [8]. The aim of the present paper is to put forward a short description of the idea of the latter method and show its application in finding the optimal shapes of latticed shells, parameterized by small number of design variables being coefficients of the Bernstein polynomials used to model the overall shape of the structures. It turns out that this method compares favorably with other available global optimization methods. As to the best author's knowledge the method discussed has never been applied to structural optimization.

2. One-dimensional global optimization under non-convex constraints – short description of the index approach

The aim of this section is to recall the most important ideas of the one-dimensional global optimization method basing on Chapter 6 of the monograph [8].

Let us consider the constrained one-dimensional global minimization problem

$$\phi\left(x^*\right) = \min_{x\in[a,b]} \left\{\phi(x)\middle|\ \forall 1 \le i \le m \quad g_i(x) \le 0\right\} \tag{1}$$

where the objective function $g_{m+1} = \phi$ and constraints functions g_i $(i = 1, \ldots, m)$ are assumed to be Lipschitzian with constants L_i $(i = 1, \ldots, m, m+1)$, i.e.,

$$\forall i \in \{1, \ldots, m, m+1\} \quad \exists L_i \in (0, \infty) \quad \forall x', x'' \in [a, b] \quad \left|g_i\left(x''\right) - g_i\left(x'\right)\right| \le L_i \left|x'' - x'\right| \tag{2}$$

and, in general, are assumed to have many local minima which is characteristic for non-convex functions. Additionally we assume that each function g_i $(i = 1, \ldots, m)$ is defined and computable only in the following subinterval Q_i $(i = 1, \ldots, m, m+1)$ of the domain $[a, b]$:

$$\begin{aligned}
&g_1 :\ Q_1 \to \mathbb{R}, \quad Q_1 = [a, b]\,,\\
&g_2 :\ Q_2 \to \mathbb{R}, \quad Q_2 = \left\{x \in Q_1\middle|\ g_1(x) \le 0\right\},\\
&\vdots\\
&g_m :\ Q_m \to \mathbb{R}, \quad Q_m = \left\{x \in Q_{m-1}\middle|\ g_{m-1}(x) \le 0\right\},\\
&g_{m+1} :\ Q_{m+1} \to \mathbb{R}, \quad Q_{m+1} = \left\{x \in Q_m\middle|\ g_m(x) \le 0\right\}.
\end{aligned} \tag{3}$$

Introducing the empty set $Q_{m+2} = \emptyset$ we have the obvious inclusions:

$$[a, b] = Q_1 \supset Q_2 \supset \ldots \supset Q_{m+1} \supset Q_{m+2} = \emptyset \tag{4}$$

and we can rewrite the problem (1) as

$$\phi\left(x^*\right) = \min_{x\in Q_{m+1}} g_{m+1}(x). \tag{5}$$

For each $x \in [a, b]$, it is convenient to define the number $\nu = \nu(x)$, called index, by the relations

$$x \in Q_\nu \ \wedge\ x \notin Q_{\nu+1} \tag{6}$$

and the maximum value M of index $\nu(x)$ over $[a, b]$

$$1 \le M = \max_{x\in[a,b]} \nu(x) \le m + 1. \tag{7}$$

The introduced above notions, allow us to define an auxiliary problem

$$g_M^* = g_M\left(x_M^*\right) = \min_{x\in Q_M} g_M(x) \tag{8}$$

which always has a solution because the set Q_M is non-empty. It can be proved very easy that incompatibility of the constraints of the problem (1) (i.e. when $M < m+1$) implies $g_M^* > 0$. In the case when $M = m+1$ (a well defined problem (5)) the solution g_M^* of the problem (8) is the solution of the primary problem (5) and any three relations: $g_M^* < 0 \ \vee\ g_M^* = 0 \ \vee\ g_M^* > 0$ are possible and admissible. The main idea of Strongin and Sergeyev's approach is to rearrange the conditional problem (8) to the unconstrained problem:

$$\Phi\left(x^*\right) = \min_{x\in[a,b]} \Phi(x) \tag{9}$$

where

$$\Phi(x) = \begin{cases} g_\nu(x) & \text{for } \nu = \nu(x) < M,\\ g_\nu(x) - g_M^* & \text{for } \nu = \nu(x) = M. \end{cases} \tag{10}$$

The problems (8) and (9) have the common sets of global minimizers, since function $\Phi(x)$ is strictly positive at all points which are not a solution of (8), while it vanishes at points which are a solution. Below, the very short description of the index method of global optimization (IMGO) is presented (see [8], p. 385).

IMGO Algorithm

Rule 0. The first trial is to be carried out at an arbitrary interior point $x^1 \in (a, b)$. The choice of the point x^{k+1}, $k \geq 1$ is determined by the following rules:

Rule 1. Renumber the points $x^1, \ldots, x^k$ of the previous trials by subscripts in increasing order of the coordinate, i.e.

$$a = x_0 < x_1 < \ldots < x_i < \ldots < x_k < x_{k+1} = b \tag{11}$$

and juxtapose to them the values $z_i = g_\nu(x_i)$, $\nu = \nu(x_i)$, $1 \leq i \leq k$ computed at these points. Points $x_0 = a$, $x_{k+1} = b$ are introduced into the series (11) as the additional ones with undefined values z_0, z_1.

Rule 2. Classify all subscripts i, $1 \leq i \leq k$ in the series (11) with respect to the number of constraints met at the corresponding points x_i by constructing the sets

$$\forall \nu \in \{1, \ldots, m+1\} \quad I_\nu = \left\{ i \in \{1, \ldots, k\} \;\middle|\; \nu = \nu(x_i) \right\}. \tag{12}$$

Boundary points $x_0 = a$, $x_{k+1} = b$ are interpreted as having zero indices, i.e. $\nu(x_0) = \nu(x_{k+1}) = 0$ and their numbers constitute the set

$$I_0 = \{0, k+1\}. \tag{13}$$

Rule 3. Find the sums of the above sets

$$\begin{aligned} &S_1 = I_0, \\ &S_2 = I_0 \cup I_1, \\ &\vdots \\ &S_{m+1} = I_0 \cup I_1 \cup \ldots \cup I_{m-1} \cup I_m, \end{aligned} \tag{14}$$

and construct the sets

$$\begin{aligned} &T_1 = I_2 \cup I_3 \cup \ldots \cup I_m \cup I_{m+1} \cup I_{m+2}, \\ &T_2 = I_2 \cup \ldots \cup I_m \cup I_{m+1} \cup I_{m+2}, \\ &\vdots \\ &T_{m+1} = I_{m+2}, \end{aligned} \tag{15}$$

where $I_{m+2} = \emptyset$.

Rule 4. Compute the running lower bounds

$$\mu_\nu = \max_{i,j \in I_\nu} \left\{ \frac{|z_i - z_j|}{x_i - x_j} \;\middle|\; i > j \right\} \tag{16}$$

for the unknown Lipschitz constants L_ν of the functions g_ν, $1 \leq \nu \leq m+1$. If the set I_ν contains fewer than two elements or if $\mu_\nu = 0$, assume that $\mu_\nu = 1$.

Rule 5. For all non-empty sets I_ν, $1 \leq \nu \leq m+1$, find the values

$$z_\nu^* = \begin{cases} \min\limits_{i \in I_\nu} z_i & \text{if } T_\nu = \emptyset, \\ 0 & \text{if } T_\nu \neq \emptyset. \end{cases} \tag{17}$$

Rule 6. For each interval (x_{i-1}, x_i), $1 \le i \le k+1$ compute the descriptor $R(i)$ as follows

$$\begin{aligned} R(i) &= \Delta_i + \frac{(z_i - z_{i-1})^2}{r_\nu^2 \mu_\nu^2 \Delta_i} - \frac{2(z_i + z_{i-1} - 2z_\nu^*)}{r_\nu \mu_\nu} && \text{if } i-1 \in I_\nu,\ i \in I_\nu \\ R(i) &= 2\Delta_i - \frac{4(z_i - z_\nu^*)}{r_\nu \mu_\nu} && \text{if } i-1 \in S_\nu,\ i \in I_\nu \\ R(i) &= 2\Delta_i - \frac{4(z_{i-1} - z_\nu^*)}{r_\nu \mu_\nu} && \text{if } i-1 \in I_\nu,\ i \in S_\nu \end{aligned} \tag{18}$$

where

$$\Delta_i = x_i - x_{i-1}, \quad 1 \le i \le k+1 \tag{19}$$

$r_\nu > 1$, $1 \le \nu \le m+1$ are the input parameters of the algorithm, which allows us, by proper choice of r_ν, to use the product $r_\nu \mu_\nu$ as an upper bound for Lipschitz coefficient L_ν.

Rule 7. Select the interval (x_{t-1}, x_t) with the maximal descriptor

$$R(t) = \max_{1 \le i \le k+1} R(i) \tag{20}$$

and execute the next trial at the middle point of the interval if the end-points indices are different, i.e.,

$$x^{k+1} = \frac{x_t + x_{t-1}}{2}, \quad \nu(x_{t-1}) \ne \nu(x_t). \tag{21}$$

Otherwise, execute the next trial at the point

$$x^{k+1} = \frac{x_t + x_{t-1}}{2} - \frac{z_t - z_{t-1}}{2r_\nu \mu_\nu}, \quad \nu(x_{t-1}) = \nu(x_t). \tag{22}$$

These rules may be appended with the termination criterion

$$x_t - x_{t-1} \le \varepsilon \tag{23}$$

where $\varepsilon > 0$ is the preassigned accuracy of search.

Theorem 1 (sufficient convergence conditions)**.** *Assume that the following conditions are satisfied:*

1. *Each domain Q_i, $1 \le i \le M$, is a finite union of positive length intervals.*
2. *Each function $g_i(x)$, $x \in Q_i$, $1 \le i \le M$, admits a Lipschitzian (with the constant L_i) extension throughout $[a, b]$, i.e., $g_i(x) = G_i(x)$, $x \in Q_i$, $1 \le i \le M$.*
3. *Since some step (i.e. if k in* (11) *is sufficiently large) the values μ_ν, $1 \le \nu \le M$ satisfy the inequalities*

$$r_\nu \mu_\nu > 2L_\nu, \quad 1 \le \nu \le M. \tag{24}$$

Then:

I. Any limit (cluster) point $\overline{x}$ of the sequence $\{x^k\}$ generated by the decision rules of the IMGO for the problem (8) *at $\varepsilon = 0$ in the termination criterion* (23) *is the solution to this problem. It is the solution to the problem* (1) *if $M = m+1$.*

II. Any point x_M^* from (8) *is the limit (cluster) point of the sequence $\{x^k\}$ generated by the IMGO.*

In monograph [8] one can find also specific methods of acceleration of the search with local tuning for solving problems with non-convex constraints, which can significantly improve effectiveness of the presented algorithm IMGO.

3. Application of the space filling curves in optimization problems with arbitrary number of design variables

Let us consider the constrained global minimization problem

$$\phi^* = \phi(\mathbf{w}^*) = \min_{w \in S} \left\{ \phi(\mathbf{w}) \,\middle|\, \forall 1 \le i \le m \quad g_i(\mathbf{w}) \le 0 \right\} \tag{25}$$

where

$$S = \left\{ \mathbf{w} = [w_1, \ldots, w_N]^{\mathrm{T}} \in \mathbb{R}^N \,\middle|\, \forall j \in \{1, \ldots, N\} \quad a_j \le w_j \le b_j \right\}. \tag{26}$$

It appears that much more convenient is to examine the following constrained global minimization problem

$$\phi^* = \phi(\mathbf{y}^*) = \min_{\mathbf{y} \in D} \left\{ \phi(\mathbf{y}) \,\middle|\, \forall 1 \le i \le m \quad g_i(\mathbf{y}) \le 0 \right\} \tag{27}$$

where

$$D = \left\{ \mathbf{y} = [y_1, \ldots, y_N]^{\mathrm{T}} \in \mathbb{R}^N \,\middle|\, \forall j \in \{1, \ldots, N\} \quad -\frac{1}{2} \le y_j \le \frac{1}{2} \right\}. \tag{28}$$

Simple transformation (see [8]) of the hyper parallelepiped S onto D allows us to keep up the domain of search (28) (which is assumed to be the standard one) instead of the domain (26).

Similarly as in (1), the objective function $g_{m+1} = \phi$ and constraints functions g_i $(i = 1, \ldots, m)$ are assumed to be Lipschitzian with constants L_i $(i = 1, \ldots, m, m+1)$, i.e.,

$$\begin{gathered} \forall i \in \{1, \ldots, m+1\} \quad \exists L_i \in (0, \infty) \quad \forall\, \mathbf{y}' = \left[y'_1, \ldots, y'_N\right]^{\mathrm{T}},\ \mathbf{y}'' = \left[y''_1, \ldots, y''_N\right]^{\mathrm{T}} \in D \\ \left| g_i(y'') - g_i(y') \right| \le L_i \left\| \mathbf{y}'' - \mathbf{y}' \right\| = L_i \sqrt{\sum_{j=1}^{N} \left| y'_j - y''_j \right|^2} \end{gathered} \tag{29}$$

and, in general, are assumed to have many local minima (non-convex functions).

A possible way to present the problem (27) by its multi-dimensional equivalent, which may be effectively solved using the techniques similar to those presented in IMGO algorithm is to employ a single-valued Hilbert-Peano curve $y = y(x)$ continuously mapping the unit interval $[0, 1]$ on the x-axis onto the hypercube (28), yielding the equality

$$\phi^* = \phi(\mathbf{y}^*) = \phi[y(x^*)] = \min_{x \in [0,1]} \left\{ \phi[y(x)] \,\middle|\, \forall 1 \le i \le m \quad g_i[y(x)] \le 0 \right\}. \tag{30}$$

A brief history of the mapping problem: interval → square

In 1878 Georg Cantor constructed the mapping

$$y : [0, 1] \to [0, 1] \times [0, 1] \subset \mathbb{R}^2 \tag{31}$$

which is injection

$$\forall x', x'' \in [0, 1] \quad x' \ne x'' \Rightarrow y(x') \ne y(x'') \tag{32}$$

and surjection

$$\forall z \in [0, 1] \times [0, 1] \quad \exists x \in [0, 1] \quad z = y(x) \tag{33}$$

(bijection from $[0, 1]$ onto $[0, 1] \times [0, 1]$). The mapping y is not continuous.

In 1890 Giuseppe Peano and in 1891 David Hilbert constructed the mapping (31) which is a continuous surjection,

$$\forall x \in [0,1] \, \forall \{x_n\} \subset [0,1] \quad \lim_{n\to\infty} x_n = x \Rightarrow \lim_{n\to\infty} y(x_n) = y(x) \tag{34}$$

but is not an injection

$$\exists x_1, x_2 \in [0,1] \quad (x_1 \neq x_2) \wedge [y(x_1) = y(x_2)] \tag{35}$$

In 1911 Luitzen Brouwer proved that a continuous mapping

$$y : [0,1] \to [0,1] \times [0,1] \subset \mathbb{R}^2 \tag{36}$$

which is injective, surjective and $y^{-1} : [0,1] \times [0,1] \to [0,1]$ is continuous does not exist.

Finally, the following definition of the space-filling curve was adopted in [8]: the single-valued continuous correspondence $y(x)$, mapping the unit interval $[0,1]$ on the x-axis onto the hypercube D from (28), is said to be Hilbert-Peano-type curve (HP curves) or space-filling curve. The various computable approximations to the HP curves were suggested in [8]. The family of the piece-wise linear mappings play the fundamental role

$$l_M : [0,1] \to D \subset \mathbb{R}^N, \quad M = 1, 2, \ldots \tag{37}$$

They map the closed interval $[0,1] \subset \mathbb{R}$ into the hypercube $D \subset \mathbb{R}^N$ including some bijections approximating the HP curve with an arbitrary accuracy dependant on the level of precision M. The construction scheme of the l_M family in $\mathbb{R}^N$, $N \geq 2$, is fairly complicated and depends on the proper linking between the two systems of numeration:

1. numeration of the family of subcubes originated in the process of division of the hypercube $D \subset \mathbb{R}^N$ into 2^{MN} subcubes with edge length equal to $\frac{1}{2^M}$,
2. numeration of the family of subintervals originated in the process of division of the closed interval $[0,1] \subset \mathbb{R}$ into 2^{MN} subintervals of length equal to $\frac{1}{2^{MN}}$.

Consider the approximation of the HP curve by the piece-wise linear mapping l_M for the least accuracy defined by $M = 1$, in two dimensional ($N = 2$) Euclidean space $\mathbb{R}^2$, see Fig. 1. In the

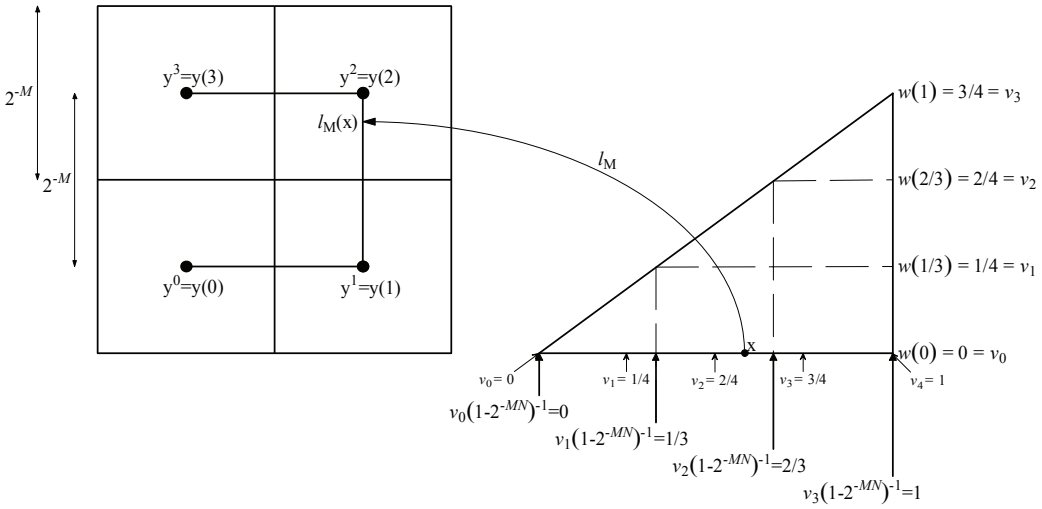

Fig. 1. The example of the approximation of the HP curve by the piece-wise linear mapping l_M in two-dimensional Euclidean space for the least accuracy $M = 1$.

left figure, the four subcubes of the first partition ($M = 1$) of the hypercube $D \subset \mathbb{R}^2$ with centers at points $\mathbf{y}^0, \mathbf{y}^1, \mathbf{y}^2, \mathbf{y}^3 \in D \subset \mathbb{R}^{N=2}$ are shown. In the right figure, the four subintervals $[\nu_0, \nu_1)$, $[\nu_1, \nu_2)$, $[\nu_2, \nu_3)$, $[\nu_3, \nu_4]$ of the first partition ($M = 1$) of the unit interval $[0, 1] \subset \mathbb{R}$ with appropriate endpoints ν_0, ν_1, ν_2, ν_3 are shown. Moreover, the graph of the linear function $w : [0, 1] \to \mathbb{R}$ is shown together with its image under the mapping l_M. Four intermediate points $\frac{\nu_0}{1-2^{-MN}}$, $\frac{\nu_1}{1-2^{-MN}}$, $\frac{\nu_2}{1-2^{-MN}}$, $\frac{\nu_3}{1-2^{-MN}}$ define three equal subintervals that are mapped on three segments $\overline{\mathbf{y}^0\mathbf{y}^1}$, $\overline{\mathbf{y}^1\mathbf{y}^2}$, $\overline{\mathbf{y}^2\mathbf{y}^3} \subset D$ being the first approximation of the HP curve in $\mathbb{R}^2$. The binary representation $\sum_{k=1}^{MN} \alpha_{ik} 2^{-k}$ of each of the point ν_i, $i = 0, 1, 2, 3$ (left-end-points) is used in coding the indices $z_1, z_2, \ldots, z_M$ identifying all subintervals designated as $d(z_1, z_2, \ldots, z_M)$. Similar notation $D(z_1, z_2, \ldots, z_M)$ is adopted for subcubes in $D \subset \mathbb{R}^N$, but identification of the adjacent subcubes together with their numeration is not trivial and requires the mathematical formulae answering the questions "when the vector $(z'_1, z'_2, \ldots, z'_M)$ precedes the vector $(z''_1, z''_2, \ldots, z''_M)$" and "when the corresponding subcubes $D(z'_1, z'_2, \ldots, z'_M)$, $D(z''_1, z''_2, \ldots, z''_M)$ are adjacent" in the sense of the precedence relation.

The space-filling curve $y : [0, 1] \to D$ refers to the approximation $l_M : [0, 1] \to D$ as a limit object emerging in sequential constructions of l_M for $M \to \infty$. It is very important that the correspondence $y = y(x)$ fulfils the following condition:

$$\forall M \geq 1 \quad \forall x \in [0, 1] \quad y(x) \in D(z_1, \ldots, z_M) \Leftrightarrow x \in d(z_1, \ldots, z_M). \tag{38}$$

Theorem 2. *Each mapping $y : [0, 1] \to D$ that fulfils condition* (38) *has the following properties:*

1. *$y = y(x)$ is the space-filing curve (HP curve).*
2. *If $g : D \to \mathbb{R}$ is Lipschitzian with some constant $L > 0$*

$$\forall\, \mathbf{y}' = \left[y'_1, \ldots, y'_N\right]^{\mathrm{T}},\ \mathbf{y}'' = \left[y''_1, \ldots, y''_N\right]^{\mathrm{T}} \in D \quad \left|g\left(\mathbf{y}''\right) - g\left(\mathbf{y}'\right)\right| \leq L \left\|\mathbf{y}'' - \mathbf{y}'\right\|, \tag{39}$$

then the univariate function $g \circ y : [0, 1] \to \mathbb{R}$ satisfies the following Hölder condition

$$\forall x', x'' \in [0, 1] \quad \left|g\left[y\left(x'\right)\right] - g\left[y\left(x''\right)\right]\right| \leq 2L\sqrt{N+3}\left|x' - x''\right|^{\frac{1}{N}}. \tag{40}$$

In particular, this fact implies that the function $\phi \circ y : [0, 1] \to \mathbb{R}$ in (30) is not Lipschitzian and satisfies the Hölder condition

$$\forall x', x'' \in [0, 1] \quad \left|\phi\left[y\left(x'\right)\right] - \phi\left[y\left(x''\right)\right]\right| \leq 2\, L\, \sqrt{N+3}\ \left|x' - x''\right|^{\frac{1}{N}} \tag{41}$$

which enforces some necessary modifications in IMGO algorithm for finding the global minimum $\mathbf{y}^* = y(x^*) \in D$, $x^* \in [0, 1]$ of the function $\phi[y(x)]$ instead of the function $\phi(\mathbf{y})$.

Another important fact should be noticed that it is not possible to calculate the values of the function $\phi[y(x)]$ because we have at our disposal only approximations of the HP curve $y(x)$, e.g. Hilbert-Peano-like piecewise-linear evolvent l_M. This fact implies the obvious suggestion that the one and only possible solution of the problem (30) can base at most on the approximation of the HP curve, e.g. l_M for some, sufficient big value $M \geq 1$. Replacing of the problem (30) with the problem

$$\phi^* = \phi(\mathbf{y}^*) = \phi[l_M(x^*)] = \min_{x \in [0,1]} \left\{\phi[l_M(x)] \;\middle|\; \forall 1 \leq i \leq m \quad g_i[l_M(x)] \leq 0\right\} \tag{42}$$

is possible (and correct) because the following theorem (see [8], p. 488) holds.

Theorem 3. *If the function $g(\mathbf{y})$, $\mathbf{y} \in D$ is Lipschitzian with the constant $L > 0$, then for each $M \geq 1$ the one-dimensional function $g \circ l_M(x)$, $x \in [0, 1]$ satisfies the uniform Hölder condition* (40)*, i.e.,*

$$\forall x', x'' \in [0, 1] \quad \left|g\left[l_M\left(x'\right)\right] - g\left[l_M\left(x''\right)\right]\right| \leq 2L\sqrt{N+3}\left|x' - x''\right|^{\frac{1}{N}}. \tag{43}$$

A modified version of IMGO algorithm, called Multivariate Index Method (MIM) for functions with uniform Hölder condition (40) (in particular (43)) together with convergence conditions is presented in [8]. In the particular case of the unconstrained optimization, the following important inequality shows the relation between the solutions of two problems (30) and (42) (without constraints):

$$\min_{x\in[0,1]}\{\phi[l_M(x)]\} - \min_{x\in[0,1]}\{\phi[y(x)]\} \leq \frac{L\sqrt{N}}{2^{M+1}}. \tag{44}$$

The HP curve satisfies the Hölder condition being the counterpart of the estimate (41). It is one of sufficient conditions of convergence of the MIM algorithm. Other curves filling the domain (spirals and TV evolvents) do not satisfy this condition, which singles out the HP curve in the method considered.

The own implementation of the method of HP curve approximation l_M (also few other approximations) described in monograph [8] is possible, but it demands thorough understanding of almost all notions and proofs of the theorems used in all steps of mathematical presentation of the algorithm. On pages 499-511 of the monograph [8], the authors revealed the complete code in C++ language of the routines for computing images and inverse images for the suggested approximations to Peano curves: centers of the M-th partition hypercubes, piecewise-linear evolvents and non-univalent evolvents (some "cosmetic supplements" such as additional comments in few places of the code are yet desirable).

In Fig. 2 the five approximations $l_M$of the HP curve in $\mathbb{R}^3$ for various values of M ($M = 1 \div 5$) are shown. Visualization of the approximation of the "classical" HP curve in $\mathbb{R}^2$ is very well known and can be found in many articles or books on the theory of fractals.

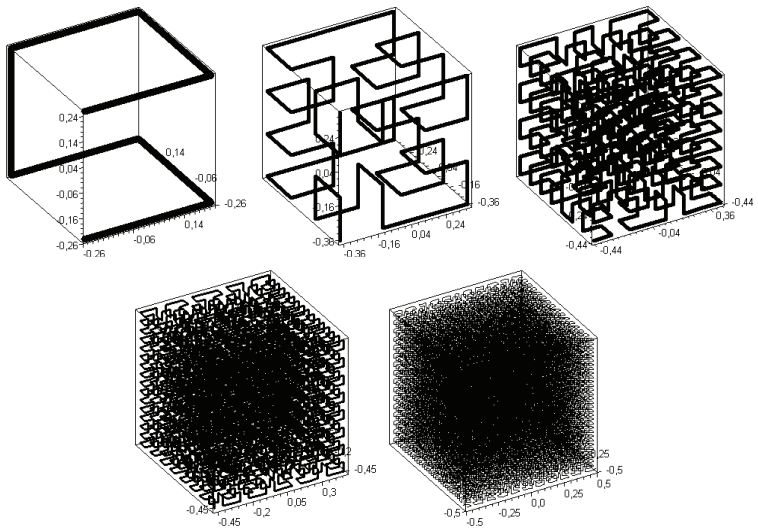

Fig. 2. The approximations l_M of the HP curve in $\mathbb{R}^3$ for values $M = 1, 2, 3, 4, 5$, respectively.

4. Truss structures. basic notation and formulation of the optimization problems

The notation used in this paragraph is independent of the notation used in two previous paragraphs.

Let $0xyz$ or $0x_1x_2x_3$ denote the global Cartesian system of coordinates. Let us consider a truss composed of M members and N nodes, subjected to the conservative nodal forces $\mathbf{Q} \in \mathbb{R}^D$ where $D = 2N$ for planar or $D = 3N$ for spatial trusses. The coordinates of nodes constitute a vector

$\mathbf{X} \in \mathbb{R}^D$. The deformation of truss structure is determined by the displacements of the nodes, which form the vector $\mathbf{q} \in \mathbb{R}^D$. The areas of cross-sections of the members form the vector $\mathbf{A} = [A_1, \ldots, A_M]^{\mathrm{T}} \in \mathbb{R}^M$. We assume that all members are made from the same linear elastic material with Young modulus E. The governing equilibrium equation for the geometrically linear case has the form

$$\mathbf{K}(\mathbf{A}, \mathbf{X})\, \mathbf{q}(\mathbf{A}, \mathbf{X}) = \mathbf{Q}. \tag{45}$$

Here,

$$\mathbf{K} = \mathbf{K}(\mathbf{A}, \mathbf{X}) = \sum_{e=1}^{M} \frac{E\, A_e}{L_e(\mathbf{X})} \mathbf{T}^e(\mathbf{X}) \otimes \mathbf{T}^e(\mathbf{X}) \in \mathbf{M}_{D\times D} \tag{46}$$

is the symmetric stiffness matrix $D \times D$,

$$L_e(\mathbf{X}) = \sqrt{\mathbf{T}^e\mathbf{X} \cdot \mathbf{X}} \tag{47}$$

denotes the length of the e-th member, the dot $(\cdot)$ implies the scalar product in $\mathbb{R}^D$. The matrices

$$\mathbf{T}^e = \mathbf{T}^e(\mathbf{X}) \in \mathbf{M}_{D\times D}, \quad e = 1, \ldots, M, \tag{48}$$

allow to express, for each e-th bar, the differences between the local Cartesian coordinates of end-nodes, by taking into account, well known in Finite Element Method (FEM), allocation matrix and using the global coordinates of nodes from vector $\mathbf{X} \in \mathbb{R}^D$ (see e.g. [1]).

The symbol $a \otimes b$ denotes the tensor product of two vectors $\mathbf{a} = [a_1, \ldots, a_D]^{\mathrm{T}}$, $\mathbf{b} = [b_1, \ldots, b_D]^{\mathrm{T}} \in \mathbb{R}^D$, or $(\mathbf{a} \otimes \mathbf{b})_{ij} = a_i\, b_j$.

The boundary conditions in (45) and (46) should be properly introduced according to the standard procedures of FEM.

In the presented examples, the shape of the undeformed shell bar structures (coordinates of the nodes) were parameterized by the two curvilinear coordinates $\left(u^1, u^2\right)$ as arguments of the three scalar functions $\varphi^i\left(u^1, u^2\right)$, $i = 1, 2, 3$, generating the position vector

$$\mathbf{r}(u^1, u^2) = \sum_{i=1}^{3} x^i \mathbf{e}_i = \sum_{i=1}^{3} \varphi^i(u^1, u^2)\, \mathbf{e}_i \tag{49}$$

where $\{\mathbf{e}_1, \mathbf{e}_2, \mathbf{e}_3\}$ denotes the orthonormal base of the global Cartesian coordinate system.

The axial symmetrical problems to be discussed will be considered within the following conventional parameterizations

- the global Cartesian parameterizations:

$$\left(u^1, u^2\right) = (x, y)\,, \quad x^1 = x, \quad x^2 = y, \quad x^3 = \varphi(x, y); \tag{50}$$

- the spherical parameterizations:

$$\left(u^1, u^2\right) = (\theta, z)\,, \quad x^1 = r(\gamma)\cos\gamma\cos\theta, \quad x^2 = r(\gamma)\cos\gamma\sin\theta, \quad x^3 = r(\gamma)\sin\gamma; \tag{51}$$

- the cylindrical parameterizations:

$$\left(u^1, u^2\right) = (\theta, z)\,, \quad x^1 = r(z)\cos\theta, \quad x^2 = r(z)\sin\theta, \quad x^3 = z. \tag{52}$$

The functions $\varphi = \varphi(x, y)$, $r = r(\gamma)$, $r = r(z)$ will be expressed in terms of the design variables.

The design variables of the truss structures can be represented by vector $\mathbf{A}$ (topology optimization), vector $\mathbf{X}$ (geometry optimization) or vectors $\mathbf{A}$ and $\mathbf{X}$ together (simultaneous topology and geometry optimization). Number of unknowns can be significantly reduced in the case of geometry optimization if the positions of nodes represented by vector $\mathbf{X}$ are dependent on just few parameters, e.g., on unknown coefficients of Bernstein polynomials. In the case of axial symmetrical, spherical or cylindrical latticed shells we can assume that

$$r(\gamma) = B_n(\gamma) = \sum_{0 \le i \le n} r_n^i \frac{n!}{i!\,(n-i)!} \left(\frac{\gamma - \gamma_a}{\gamma_b - \gamma_a}\right)^i \left(1 - \frac{\gamma - \gamma_a}{\gamma_b - \gamma_a}\right)^{n-i} \tag{53}$$

or

$$r(z) = B_n(z) = \sum_{0 \le i \le n} r_n^i \frac{n!}{i!\,(n-i)!} \left(\frac{z - z_a}{z_b - z_a}\right)^i \left(1 - \frac{z - z_a}{z_b - z_a}\right)^{n-i} \tag{54}$$

where $n \ge 1$ denotes the fixed degree of the Bernstein polynomial, r_n^i, $0 \le i \le n$, are unknown coefficients – design variables, γ_a, γ_b ($\gamma_a < \gamma_b$), or z_a, z_b ($z_a < z_b$), are lower and upper limits for angle γ ($\gamma_a \le \gamma \le \gamma_b$), and vertical coordinate z ($z_a \le z \le z_b$) in spherical and cylindrical latticed shells, respectively.

In the case of Cartesian coordinate system we can similarly assume that

$$\begin{aligned} \varphi(x, y) = \sum_{0 \le i \le n} \sum_{0 \le j \le n} \varphi_n^{ij} \frac{n!}{i!\,(n-i)!} \frac{n!}{j!\,(n-j)!} \left(\frac{x - x_a}{x_b - x_a}\right)^i \left(\frac{y - y_a}{y_a - y_b}\right)^i \\ \cdot \left(1 - \frac{x - x_a}{x_b - x_a}\right)^{n-i} \left(1 - \frac{y - y_a}{y_a - y_b}\right)^{n-i}. \end{aligned} \tag{55}$$

Here, φ_n^{ij}, $0 \le i, j \le n$, are unknown coefficients – design variables, x_a, x_b ($x_a < x_b$) and y_a, y_b ($y_a < y_b$) are lower and upper limits for coordinates x ($x_a \le x \le x_b$) and y ($y_a \le y \le y_b$). The real number of design variables will be even less then $n + 1$ or $(n + 1)^2$ because bottom or bottom and top coordinates of nodes of axial symmetrical spherical and cylindrical latticed shells could be treated as constant, similarly as the four extreme edges of latticed shells defined in Cartesian coordinate system. So, we could have only n, $n - 1$ or $(n - 1)^2$ real design variables describing the optimal shape of the latticed shells. It is worth to notice that in such way defined variables allow us to keep the axial symmetry of the shape of the latticed shell both before optimization as well upon optimization even in the case of asymmetrical loading (modeling, e.g., the wind load) and no vector optimization is needed.

All presented examples (except the first one) of the optimization of trusses refer to compliance optimization with only one functional constraint on entire volume of the bars (limitation on weight of the structure). The problems will assume the form

$$\phi^* = \phi(\mathbf{w}^*) = \min_{\mathbf{w} \in S} \left\{ \phi(\mathbf{w}) \,\middle|\, g_1(\mathbf{w}) \le 0 \right\} \tag{56}$$

where the vector $\mathbf{w}$ of design variables will have one of the forms:

$$\begin{aligned} &\mathbf{w} = \mathbf{A}, \quad \text{or} \quad \mathbf{w} = \mathbf{X}, \quad \text{or} \quad \mathbf{w} = [\mathbf{A}, \mathbf{X}]^{\mathrm{T}}, \\ &\text{or} \quad \mathbf{w} = \mathbf{U} = \left[\ldots, r_n^i, \ldots\right]^{\mathrm{T}}, \quad \text{or} \quad \mathbf{w} = \mathbf{U} = \left[\ldots, r_n^{ij}, \ldots\right]^{\mathrm{T}}. \end{aligned} \tag{57}$$

The objective function (compliance) $\phi = \phi(\mathbf{w})$ is defined as

$$\phi : S \to \mathbb{R}, \quad \phi(\mathbf{w}) = \mathbf{Q} \cdot \mathbf{q}(\mathbf{w}) \tag{58}$$

where $\mathbf{q} = \mathbf{q}(\mathbf{w})$ is the solution of the equilibrium equation (45), or

$$\mathbf{q}(\mathbf{w}) = \mathbf{K}^{-1}(\mathbf{w})\,\mathbf{Q}. \tag{59}$$

The constraint function $g_1 = g_1(\mathbf{w})$ is defined as

$$g_1 : S \to \mathbb{R}, \quad g_1(\mathbf{w}) = \sum_{e=1}^{M} L_e(\mathbf{X})\,A_e - V_0 \tag{60}$$

where V_0 represents the upper limit volume (most often assumed as multiple of initial volume V_{init} of the truss, e.g. equal to $2V_{\text{init}}$). The simple box constraints defining the cube S in (56) depend on type of the choice of vector $\mathbf{w}$.

No sensitivity analysis is necessary in classical versions of the global optimization algorithms presented in monograph [8], but in some examples, the gradient-based Method of Moving Asymptotes (MMA) [9] were additionally applied. Necessary formulae on gradients of the functions ϕ and g_1 can be found, e.g., in [1].

5. Case studies

The described in Secs. 2 and 3 method MIM was implemented in optimization problems of truss structures. The program including the MIM method and statics of trusses was written in C++ language. There were used functions for computing images and inverse images for the HP curves from [8] (own routines proved to be correct but less numerically effective).

5.1. Statically indeterminate, plane three bar truss

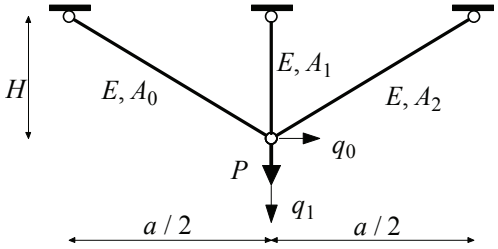

Fig. 3. Weight optimization of the three bar truss

In this example (see Fig. 3) we consider the problem of weight minimization of the symmetric, planar three bar truss

$$\min_{A\in\mathbb{R}^3, H\in\mathbb{R}} \left\{ \rho\mathbf{A}\cdot\mathbf{L}\,(H) \;\middle|\; \mathbf{A}_{\min} \le \mathbf{A} \le \mathbf{A}_{\max}, \quad H_{\min} \le H \le H_{\max}, \quad \boldsymbol{\sigma} \le \boldsymbol{\sigma}_{\max}, \quad q_1 \le q_{\max} \right\} \tag{61}$$

with box constraints on cross sections of three bars

$$5.0\cdot 10^{-5}\left[\mathrm{m}^2\right] = A_{\min} \le A_e \le A_{\max} = 2.0\cdot 10^{-4}\left[\mathrm{m}^2\right], \quad e = 0, 1, 2, \tag{62}$$

and height of the truss

$$0.3\,[\mathrm{m}] = H_{\min} \le H \le H_{\max} = 0.7\,[\mathrm{m}]\,. \tag{63}$$

In Eq. (61) ρ denotes density of the material, $\boldsymbol{\sigma} \in \mathbb{R}^M$ denotes the vector of stresses in bars. Inequalities "$\le$" used for the vector quantities should be understood as component wise.

Functional constraints concern stresses in three bars

$$\sigma_e = \frac{E}{L_e(\mathbf{X})^2}\mathbf{T}^e\mathbf{X}\cdot\mathbf{q} \leq \sigma_{\max} = 100.0\,[\mathrm{MPa}]\,, \quad e = 0,1,2, \tag{64}$$

and vertical displacement of the node

$$q_1 \leq q_{\max} = 5.0\cdot 10^{-3}\,[\mathrm{m}]\,. \tag{65}$$

Remaining data are:

$$a = 1.0\,[\mathrm{m}]\,, \quad E = 7.1\cdot 10^4\,[\mathrm{MPa}]\,, \quad P = 1.0\cdot 10^4\,[\mathrm{N}]\,, \quad \rho = 2.8\cdot 10^3\,\left[\mathrm{kg/m^3}\right]. \tag{66}$$

The initial values of the design variables are as follows:

$$A_0 = A_1 = A_2 = 1.0\cdot 10^{-4}\,\left[\mathrm{m^2}\right], \quad H = 0.5\,[\mathrm{m}]\,, \tag{67}$$

and the initial value of the weight is

$$W_{\mathrm{init}} = 0.53598\,[\mathrm{kg}]\,. \tag{68}$$

The optimal values of the design variables obtained from MIM are:

$$A_0 = A_2 = 5.0\cdot 10^{-5}\,\left[\mathrm{m^2}\right], \quad A_1 = 8.635\cdot 10^{-5}\,\left[\mathrm{m^2}\right], \quad H = 0.30003319\,[\mathrm{m}]\,. \tag{69}$$

and the optimal value of the weight is

$$W_{\mathrm{opt}} = 0.23581\,[\mathrm{kg}]\,. \tag{70}$$

The solution is 0.01 times better than the best known (for the present author) solution [10]:

$$A_0 = A_2 = 5.05\cdot 10^{-5}\,\left[\mathrm{m^2}\right], \quad A_1 = 8.7\cdot 10^{-5}\,\left[\mathrm{m^2}\right], \quad H = 0.3001\,[\mathrm{m}] \tag{71}$$

with the optimal weight:

$$W_{\mathrm{opt}} = 0.239\,[\mathrm{kg}]\,. \tag{72}$$

5.2. A cylindrical latticed shell as a simplified truss model of a multi-storeyed building

Are the tulip like shapes of the high-rise, multi-storeyed buildings, proposed few years ago by well known architects and structural engineers (see, e.g., W. Zabłocki [11, 13] and W. Zalewski [12, 13]) the counterparts of the Michell-Hemp cantilever (see [2]) in three dimensions? Several projects of such buildings were already realized, e.g.. 30 St Mary Axe, also known as the Gherkin and the Swiss Re Building, is a skyscraper in London's main financial district, the City of London, completed in December 2003 and opened on 28 April 2004. It is 180 meters tall, with 40 floors (see Fig. 4). The exact mathematical solutions being three-dimensional counterparts of the well known exact solution in two-dimension are unknown. So, the numerical simulations can only give partial answers to the above question. The very simplified truss model of a such skyscraper is defined in such a way that Cartesian pattern, defined in Fig. 5, is projected onto a cylindrical layout of the latticed shell (envelope structure). The horizontal forces are assumed to be put at all top nodes while all bottom nodes are supported ("spatial counterpart" of Michell's cantilever).

Initial data are the height and radius of the cylinder: $H = 185.0\,[\mathrm{m}]$, $R = 30.0\,[\mathrm{m}]$, respectively. The area of each cross section and Young modulus of the bars are: $A_e = 0.1\,\left[\mathrm{m^2}\right]$ and $E = 1.0\cdot 10^9\,\left[\mathrm{N/m^2}\right]$. The value of each horizontal force put at the top node of the cylinder is $Q_i = 3000.0\,[\mathrm{N}]$.

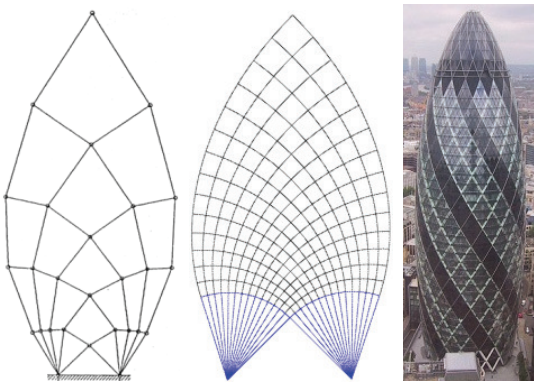

Fig. 4. Sketch of the Michell-Hemp cantilever in two dimensions and skyscraper 30 St Mary Axe in London (`http://en.wikipedia.org/wiki/File:30_St_Mary_Axe,_%27Gherkin%27.JPG`)

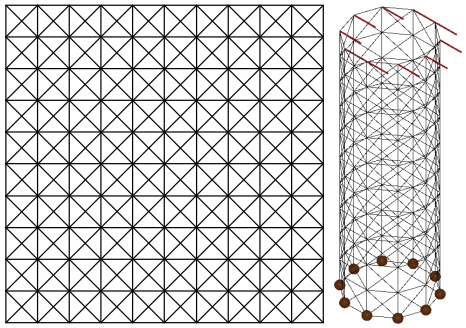

Fig. 5. Simplified model of a skyscraper as a cylindrical latticed shell

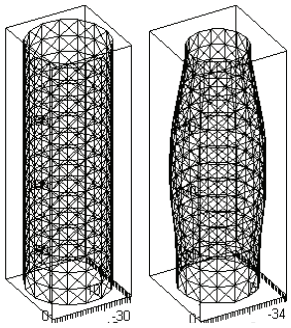

Fig. 6. Initial and optimal shape of the cylindrical latticed shell emulating three-dimensional counterpart of the Michell cantilever.

Project parameters were defined according to (54) for degree $n = 8$ of Bernstein polynomial (real number of parameters = 7).

Level M in (37) of accuracy of the HP curve approximation: $M = 6$. The values of the radius R of the axial symmetrical structure can change from 20 [m] to 50 [m]. The initial compliance is $\phi = 240772$ [Nm], and the optimal compliance equals: $\phi^* = 235888$ [Nm]. The initial and optimal shape of the latticed shell is shown in Fig. 6.

The optimal shape can clearly motivate the tulip like shapes of the high-rise building in the proposed model of latticed shell. The reduction of compliance (increase of stiffness) is not so big as in the case of classical plane Michell cantilever but the shape of a great deal of trees and many other plants nearing cylindrical one suggests that its modifications and improvement has significantly limited range.

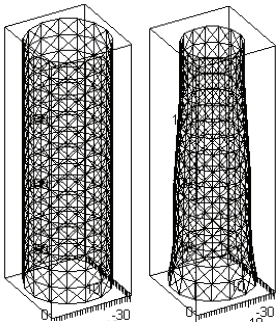

Fig. 7. Initial and optimal shape of the cylindrical latticed shell emulating three-dimensional counterpart of the Michell cantilever with additional vertical loading put at each top node..

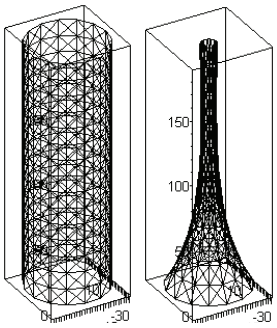

Fig. 8. Initial and optimal shape of the cylindrical latticed shell with only vertical loading applied to all nodes.

Similar numerical simulation with more realistic additional vertical loading $Q_i = 10000.0\,[\mathrm{N}]$ put at each top node and for diminished degree of Bernstein polynomial from $n = 8$ to $n = 5$ (real number of parameters = 4) with augmented level M in (37) of accuracy of the HP curve approximation from $M = 6$ to $M = 13$ produces the desired effect of optimal shape shown in Fig. 7. In this case the optimal compliance is equal to $\phi^* = 388107\,[\mathrm{Nm}]$ in compare with the initial one equal to $\phi = 401916\,[\mathrm{Nm}]$.

Another numerical simulation relies on replacing the loading only with vertical forces $Q_i = 1000.0\,[N]$ put at all nodes of the truss (simplified model of the weight of the structure). The values of the radius R of the axial symmetrical structure can change from $5\,[\mathrm{m}]$ to $35\,[\mathrm{m}]$. Other parameters remain the same. The initial compliance is $\phi = 1611\,[\mathrm{Nm}]$, whereas the optimal compliance equals to $\phi^* = 1124\,[\mathrm{Nm}]$. The initial and optimal shape of the cylindrical shell bar structure is shown in Fig. 8.

The following numerical simulation relating cylindrical latticed shell was performed on the base of the following data of loading and boundary condition: the horizontal forces $Q_i = 1000.0\,[N]$ are put at all nodes of the cylinder with additionally supported nodes at its top (truss model of fully clamped vertical beam). The values of the radius R of the axial symmetrical structure can change from $10\,[\mathrm{m}]$ to $50\,[\mathrm{m}]$. The degree of Bernstein polynomial $n = 6$ (real number of parameters = 4). Other parameters remain the same. The initial compliance is $\phi = 1931\,[\mathrm{Nm}]$ and the optimal compliance equals to $\phi^* = 1647\,[\mathrm{Nm}]$. The initial and optimal shape of the cylindrical latticed shell is shown in Fig. 9.

In the last numerical simulation relating cantilever cylindrical latticed shell was performed on the assumption that the loading emulates the torque at the top of the structure. The simulation mimics Michell's grid sphere with finite number of bars for which the exact solution is known (see e.g. [1, 5, 7]). But our example refers only to the shape of the truss – not to the cross sections of the bars (we perform in this case only geometry – not topology optimization). A torque is replaced by

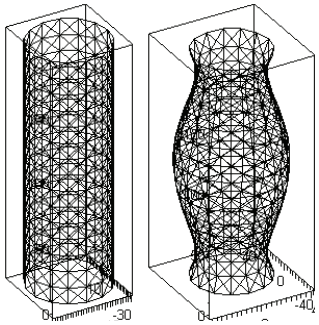

Fig. 9. Initial and optimal shape of the cylindrical latticed shell clamped on both: top and bottom horizontal rings with only horizontal loading put at all nodes.

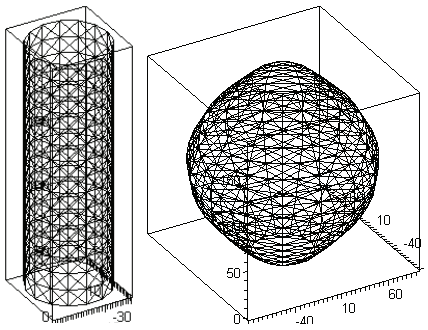

Fig. 10. Initial and optimal shape of the cantilever cylindrical latticed shell with torque emulated by tangent horizontal, concentrated forces applied to the top nodes of the truss.

"tangent" horizontal, concentrated forces $Q_i = 1000.0\,[N]$ applied to the top nodes of the truss. The degree of Bernstein polynomial $n = 6$ (real number of parameters = 4). Level M in (37) of accuracy of the HP curve approximation: $M = 13$. The values of the radius R of the axial symmetrical structure can change from 28 [m] to 100 [m]. The initial compliance is $\phi = 40.7884\,[\mathrm{Nm}]$, whereas the optimal one equals to $\phi^* = 14.7942\,[\mathrm{Nm}]$. The initial and optimal shape of the cylindrical latticed shell is shown in Fig. 10.

It is worth to notice, that the optimal – nearly spherical shape – only confirms well known analytical solution [5]. The reduction of compliance (increase of stiffness) is here much bigger than in the first simulation performed on the "cylindrical latticed shell" modelling the "3D version" of the Michell's cantilever. Additional topology optimization performed together with the above geometry optimization would certainly result in nearly exact solution (see also [1]).

5.3. Elliptic paraboloidal grid shell

In the last example we consider the elliptic paraboloidal latticed shell (width $\times$ length $= 50 \times 50\,[\mathrm{m}]$, rise of arch $= 11\,[\mathrm{m}]$) with the nodes at all edges fixed and vertical forces $Q_i = 1.0 \cdot 10^4\,[N]$ assumed to be put at all nodes.

The degree of Bernstein polynomial $n = 5$ (real number of parameters = 9). Level M in (37) of accuracy of the HP curve approximation: $M = 6$. All "internal" nodes can change only vertical positions in the range: $7.0 \div 30.0\,[\mathrm{m}]$.

The initial compliance equals $\phi = 79980\,[\mathrm{Nm}]$ and the optimal compliance is $\phi^* = 8000\,[\mathrm{Nm}]$. The initial and optimal shape of the latticed shell is shown in Fig. 11. The reduction of compliance (increase of stiffness) is here the biggest in compare with all presented previous examples.

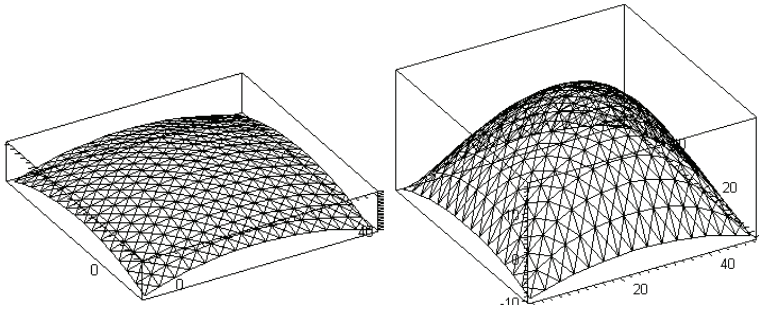

Fig. 11. Initial and optimal shape of the elliptic paraboloidal latticed shell subjected to constant vertical forces at all nodes.

6. Final remarks

Presented results were obtained by the present author as a result of his first implementation (working version) of the MIM method of global optimization elaborated by Strongin and Sergeyev in [8]. This numerical code is still developed and the presented numerical results should be treated mainly as an illustration of its potential range of application in mechanics (almost all problems were additional solved using Svanberg's gradient-base MMA [9] method that gave similar results). The approach proposed is suitable in the case of arbitrary non-convex optimization problems with arbitrary number of non-convex functional constraints. The sensitivity analysis in the most of the presented in [8] various versions of global optimization algorithms is not necessary, but it is also possible to implement additional information about gradients of the functions to increase the effectiveness of the proposed methods. The main disadvantage of the MIM method (and others) is its efficiency being significantly lower in the case of six and more design variables for which the obtained "optimal minima" should be treated rather as the sub-optimal solutions than global ones. The authors of [8] write on p. 500: "*... as long as the expansion* $x = \sum_{k=1}^{MN} \alpha_{ik} 2^{-k}$ (see text before Eq. (38) *requires* MN *binary digits, it has to be mentioned that there is the constraint* $MN < 56$ *imposed by the type double in presentation of* x *...*". This limitation does not matter in computers with arbitrary capacity of RAM and registers in processors, but nowadays it is still a serious restriction. Another disadvantage in MIM method is a difficulty in the proper choice of counterparts of input parameters $r_\nu > 1$, $1 \leq \nu \leq m+1$ that were defined in (18) for IMGO method. The values of parameters r_ν should guarantee the satisfaction of the inequalities of the type (24) since some step of the IMGO method. This is one from some other conditions that suffices for the fulfilment of the convergence criteria. As significant increase of the values of r_ν (e.g. $r_\nu \gg 2$) – theoretically safe, is rather not a good practice, as many tests have shown, from the numerical point of view. However, the proper defined values r_ν very often produced not only much more accurate results (true global minima) that was also found very often in much more shorter time. Similar comments apply to few other coefficients in MIM method (not presented in the paper).

Summing up, the whole arsenal of methods of global optimization presented in [8] should deserve the highest attention of scientists working in any field of optimization, mainly on account of solid mathematical foundations of the proposed algorithms. In the nearest future, MIM method will be implemented by the present author in designing the desirable local properties of the Hooke tensor in the so called free material design of the elastic bodies.

References

[1] S. Czarnecki. Compliance optimization of the truss structures. *Computer Assisted Mechanics and Engineering Sciences*, **10**: 117–137, 2003.

[2] C. Graczykowski, T. Lewiński. Michell cantlilevers constructed within trapezoidal domains. Part I: geometry of Hency nets. *Struct. Multidisc. Optim.*, **32**: 347–368, 2006.

[3] E. Hansen, G.W. Walster. *Global Optimization Using Interval Analysis.* Marcel Dekker, Inc., New York, 2004.

[4] H.T. Jongen, P. Jonker, F. Twilt. *Nonlinear Optimization in Finite Dimensions. Morse Theory, Chebyshev Approximation, Transversality, Flows, Parametric Aspects*. Kluwer Academic Publishers, London, 2000.
[5] T. Lewiński. Michell structures formed on surfaces of revolution. *Struct. Multdisc. Optim.*, **28**: 20–30, 2004.
[6] Z. Michalewicz. *Genetic Algorithms + Data Structures = Evolution Programs*. Springer-Verlag, Berlin, 1996.
[7] A. Michell. The limits of economy of material in frame structures. *Phil. Mag.*, **8**: 589–597, 1904.
[8] R.G. Strongin, Y.D. Sergeyev. *Global Optimization with Non-Convex Constraints*. Kluwer Academic Publishers, London, 2000.
[9] K. Svanberg. The method of moving asymptotes – a new method for structural optimization. *Int. J. Num. Meth. Eng.*, **24**: 359–373, 1987.
[10] Wahyu Kuntjoro, Jamaluddin Mahmud. Truss structural configuration optimization using the linear extended interior penalty function method. *ANZIAM J.*, **46**(E): 1311–1326, 2006.
[11] W. Zabłocki. Optimization of structures and new architectural forms of tall buildings (in Polish). *Architektura*, **74**: 96–98, 2000.
[12] W. Zalewski. The strength and the lightness – the muses of a structural engineer (in Polish). *Architektura*, **74**: 94–95, 2000
[13] W. Zalewski, W. Zabłocki. Skyscrapers. Engineering inspiration of forming the multi-storey buildings (in Polish). *Magazyn budowlany*, **8**: 50–54, 1999.